Transverse electric and transverse magnetic pulsed-beam decomposition of time-dependent aperture fields

Timor Melamed,* Dor Abuhasira, and David Dayan

Department of Electrical and Computer Engineering, Ben-Gurion University of the Negev, Beer Sheva 84105, Israel
*Corresponding author: timormel@ee.bgu.ac.il

The present contribution is concerned with applying beam-type expansion to a planar aperture time-dependent (TD) electromagnetic field in which the propagating elements, the electromagnetic pulsed-beams, are *a priori* decomposed into transverse electric (TE) and transverse magnetic (TM) field polarizations. The propagating field is described as a discrete superposition of tilted, shifted, and delayed TE and TM electromagnetic pulsed-beam propagators over the frame spectral lattice. These waveobjects are evaluated by using TD plane-wave spectral representations. Explicit asymptotic expressions for electromagnetic isodiffracting pulsed-quadratic beam propagators are presented, as well as a numerical example. © 2012 Optical Society of America

OCIS codes: 1350.5500, 050.5082, 070.2580, 080.2720, 260.1960.

1. INTRODUCTION

Beam-type (phase-space) field expansion schemes have been the subject of an intense research in the past two decades for scalar time-harmonic (TH) [1–5] and for time-dependent (TD) fields [6–10]. In general, phase-space methods for propagating in free space are not more accurate nor faster than plane-wave propagation or Green's function methods. Nevertheless, these methods are considered as a generic tool for scattering problems or for propagation in complex environments, where other methods fail. Closed-form solutions for beam propagators that are required for the expansions have been derived in homogeneous [11–13], anisotropic [14–18], dispersive [19–21], and inhomogeneous media [22–28]. Beam-type expansion methods have been applied for the analysis of large reflector antennas [29–31], for rough surface scattering [32–35], and for various inverse scattering applications [36–42].

This paper as well as its TH counterpart in [43] are based on the frame-based ultrawideband (UWB) beam summation method, which were introduced for scalar TH and TD wave fields in counterparts [3] and [8], respectively. In [3], the TH field is expressed as a sum of beams emerging from a sparse discrete set of points and directions in the source domain, as in the conventional Gabor-type representation. However, in the frame-based method, the frame overcompleteness is utilized to construct a frequency-independent lattice of beam initiation points and directions such that only one set of beams needs to be traced in the medium and then used for all frequencies. Furthermore, the method utilizes isodiffracting (ID) beam propagators [44] whose propagation parameters are frequency independent so that they can be calculated only once and then used for all frequencies. These frequency independence properties of the TH representation in [3] have been utilized in [8] to formulate a pulsed-beam (PB) representation directly in the time domain. It has been established there that the ID PBs constitute a new frame-set that was termed the windowed Radon transform (WRT) frame.

Recently the scalar field expansions were extended to include electromagnetic fields by introducing exact frame-based expansions of planar aperture TH [45] and TD [46] EM fields. In [46] the TD EM field is described as a discrete superposition of tilted, shifted, and delayed EM PB propagators over the frame spectral lattice. The propagating waveobjects are solutions of Maxwell's equations that exhibit spatial and temporal localization. A TH EM frame-based expansion was introduced in [43] in which the EM field was *a priori* decomposed into transverse electric (TE) and transverse magnetic (TM) wave polarizations, by processing the transverse aperture field components into novel TE and TM (with respect to constant z planes) EM beam-type waveobjects. The present investigation extends the TH representation in [45] for TD EM aperture fields and introduces the TE/TM EM PB propagators, which are required for the exact expansion as well as their asymptotic evaluation.

The paper outline is as follows: in Section 2 a brief description of TE and TM plane-wave decomposition of TD aperture fields is given. A review of the general formulation of the scalar TD frame-based beam decomposition is outlined in Subsection 3.A with the necessary extensions that are required for the present investigation. The special case of ID pulsed-quadratic windows is discussed in Subsection 3.B. In Section 4 the EM field is decomposed into TE/TM EM PB propagators over the frame five-dimensional spatial-directional-temporal lattice as well as the corresponding asymptotic expressions for the EM PB propagators. Finally, a numerical example that demonstrates the TE/TM EM PB expansion is given in Section 5.

2. TRANSIENT PLANE-WAVE DECOMPOSITION

We are concerned with obtaining a discrete exact PB spectral representation for the TD EM field in $z \geq 0$ due to sources in $z < 0$, given the transverse TD electric field components over $z = 0$ plane

$$\mathbf{E}_t(\mathbf{r}_t, t) = E_x(\mathbf{r}_t, t)\hat{\mathbf{x}} + E_y(\mathbf{r}_t, t)\hat{\mathbf{y}}, \qquad (1)$$

where $\hat{\mathbf{x}}$ and $\hat{\mathbf{y}}$ are the conventional Cartesian unit vectors and $\mathbf{r}_t = (x, y)$ denotes the transverse coordinates. We use the conventional Cartesian coordinate system in which the configuration space is described by $\mathbf{r} = (x, y, z)$. A hat over a vector denotes a unit vector. The propagation medium is homogeneous with ϵ_0 and μ_0 denoting the free-space permittivity and permeability, respectively.

A. Analytic Fields

In order to gain flexibility in the derivation, we apply in this paper the analytic signal representation. This representation can accommodate the complex time shift that describes the evanescent spectrum in the time-domain plane-wave representation [see Eq. (10)], and the complex time shift which describes the off-axis PB propagators [see Eq. (43)].

Given a real field $\mathbf{E}(\mathbf{r}, t)$ that is defined for real t, the corresponding analytic field is defined by the convolution integral [47]

$$\check{\mathbf{E}}(\mathbf{r}, t) = \frac{-1}{\pi j} \int_{-\infty}^{\infty} dt' \frac{\mathbf{E}(\mathbf{r}, t')}{t - t'}, \qquad \mathrm{Im}\, t \geq 0. \qquad (2)$$

Here and henceforth, analytic fields are denoted by a breve mark (˘). The limit of the analytic field on the real t axis is related to the real field $\mathbf{E}(\mathbf{r}, t)$ by

$$\check{\mathbf{E}}(\mathbf{r}, t) = \mathbf{E}(\mathbf{r}, t) - j\mathcal{H}_t \mathbf{E}(\mathbf{r}, t), \qquad t \text{ real}, \qquad (3)$$

where $\mathcal{H}_t = \mathcal{P}(1/\pi t) \bigotimes$ is the Hilbert transform operator, with $\mathcal{P}$ denoting Cauchy's principal value and $\bigotimes$ denoting a temporal convolution. Therefore, the real field for real t is recovered from the analytic field via

$$\mathbf{E}(\mathbf{r}, t) = \mathrm{Re}\, \check{\mathbf{E}}(\mathbf{r}, t). \qquad (4)$$

Note that though the physical time is real, the *time argument* of an analytic field can be complex [see, for example, Eq. (10)]. Alternatively, the analytic field $\check{\mathbf{E}}(\mathbf{r}, t)$ can be obtained by applying a one-sided (positive frequencies) inverse Fourier transform to the spectral (frequency domain) distribution of the real field $\mathbf{E}(\mathbf{r}, t)$. Because the present contribution is concerned with a direct time-domain derivation, this approach is not investigated here.

B. Time-Dependent Plane-Wave Representation

The analytic TD plane-wave spectral distribution

$$\check{\tilde{\mathbf{E}}}_t(\boldsymbol{\kappa}_t, \tau) = \check{\tilde{E}}_x(\boldsymbol{\kappa}_t, \tau)\hat{\mathbf{x}} + \check{\tilde{E}}_y(\boldsymbol{\kappa}_t, \tau)\hat{\mathbf{y}}, \qquad (5)$$

of the TD aperture field over the $z = 0$ plane, $\check{\mathbf{E}}_t(\mathbf{r}_t, t)$, is defined by [7,48]

$$\check{\tilde{\mathbf{E}}}_t(\boldsymbol{\kappa}_t, \tau) = \int d^2 r_t \check{\mathbf{E}}_t(\mathbf{r}_t, \tau + c^{-1}\boldsymbol{\kappa}_t \cdot \mathbf{r}_t), \qquad (6)$$

where $\boldsymbol{\kappa}_t = (\kappa_x, \kappa_y)$ are the directional spectral variables, τ denotes the temporal spectral variable, and c denotes the speed of light in vacuum. Equation (6) is termed the slant stack transform (SST), and it is identified as a Radon transform of $\check{\mathbf{E}}_t(\mathbf{r}_t, t)$ in the three-dimensional $(\mathbf{r}_t, t)$ space, consisting

of projections of $\check{\mathbf{E}}_t(\mathbf{r}_t, t)$ along surfaces of linear delay. The SST in Eq. (6) extracts from $\check{\mathbf{E}}_t(\mathbf{r}_t, t)$ the TD plane-wave field that is propagating in a $\boldsymbol{\kappa}_t$-dependent direction [see Eq. (10)]. The inverse STT of Eq. (6) is given by [7,48]

$$\check{\mathbf{E}}_t(\mathbf{r}_t, t) = \frac{-1}{(2\pi c)^2} \int d^2 \kappa_t \partial_t^2 \check{\tilde{\mathbf{E}}}_t(\boldsymbol{\kappa}_t, t - c^{-1}\boldsymbol{\kappa}_t \cdot \mathbf{r}_t), \qquad (7)$$

where $\partial_t^2 = \partial^2/\partial t^2$.

The aperture field is propagated into $z > 0$ half-space by applying a standard plane-wave analysis. The longitudinal spectrum, which is denoted by $\check{\tilde{E}}_z$, is obtained from Gauss law $\nabla \cdot \check{\mathbf{E}} = 0$, yielding

$$\check{\tilde{E}}_z(\boldsymbol{\kappa}_t, \tau) = -(\kappa_x \check{\tilde{E}}_x + \kappa_y \check{\tilde{E}}_y)/\kappa_z, \qquad (8)$$

where

$$\kappa_z = \sqrt{1 - \kappa_x^2 - \kappa_y^2}, \qquad (9)$$

with $\mathrm{Re}\, \kappa_z \geq 0$ in the upper Riemann sheet and $\mathrm{Im}\, \kappa_z \leq 0$ over the integration contour. Thus the electric field in $z \geq 0$ is given by the plane-wave superposition

$$\check{\mathbf{E}}(\mathbf{r}, t) = \frac{-1}{(2\pi c)^2} \int d^2 \kappa_t \partial_t^2 \check{\tilde{\mathbf{E}}}(\boldsymbol{\kappa}_t, t - c^{-1}\hat{\boldsymbol{\kappa}} \cdot \mathbf{r}), \qquad (10)$$

where

$$\check{\tilde{\mathbf{E}}}(\boldsymbol{\kappa}_t, \tau) = \check{\tilde{\mathbf{E}}}_t(\boldsymbol{\kappa}_t, \tau) + \hat{\mathbf{z}}\check{\tilde{E}}_z(\boldsymbol{\kappa}_t, \tau), \qquad (11)$$

and the spectral unit vector

$$\hat{\boldsymbol{\kappa}} = (\kappa_x, \kappa_y, \kappa_z). \qquad (12)$$

The TD plane-wave representation in Eq. (10) describes the electric field $\check{\mathbf{E}}(\mathbf{r}, t)$ in terms of an angular superposition of TD EM plane-wave propagators. In the visible range where $\kappa_x^2 + \kappa_y^2 < 1$, κ_z is real and each plane-wave propagator emanates from $z = 0$ plane in the direction of the unit vector $\hat{\boldsymbol{\kappa}}$ in Eq. (12). For $\kappa_x^2 + \kappa_y^2 > 1$, the longitudinal wavenumber is imaginary with $\mathrm{Im}\, \kappa_z < 0$ along the integration contour so that the time argument in Eq. (10) has a positive imaginary part that is multiplied by z. This yields evanescent TD plane waves that decay monotonically with z.

The representation in Eq. (10) can be rewritten as a superposition of TE and TM plane-wave spectra with respect to planes of constant z [49]. To that extent, two spectral unit vectors are defined for a given spectral $\boldsymbol{\kappa}_t$. Unit vector $\hat{\mathbf{n}}(\boldsymbol{\kappa}_t)$ denotes the normal to the so-called plane of incidence, and the tangent unit vector $\hat{\mathbf{t}}(\boldsymbol{\kappa}_t) = \hat{\boldsymbol{\kappa}} \times \hat{\mathbf{n}}$. Thus,

$$\hat{\mathbf{n}}(\boldsymbol{\kappa}_t) = \kappa_t^{-1}(\kappa_y \hat{\mathbf{x}} - \kappa_x \hat{\mathbf{y}}), \qquad \hat{\mathbf{t}}(\boldsymbol{\kappa}_t) = \kappa_z \kappa_t^{-1}(\kappa_x \hat{\mathbf{x}} + \kappa_y \hat{\mathbf{y}}) - \kappa_t \hat{\mathbf{z}},$$
$$(13)$$

where $\kappa_t = \sqrt{\kappa_x^2 + \kappa_y^2}$.

The TE and TM spectral distributions are obtained by projecting the aperture spectral distribution, $\tilde{\mathbf{E}}(\boldsymbol{\kappa}_t, \tau)$, on the unit vectors in Eq. (13):

$$\breve{\mathbf{E}}(\boldsymbol{\kappa}_t, \tau) = \breve{E}^{\mathrm{TE}}(\boldsymbol{\kappa}_t, \tau)\hat{\mathbf{n}}(\boldsymbol{\kappa}_t) + \breve{E}^{\mathrm{TM}}(\boldsymbol{\kappa}_t, \tau)\hat{\mathbf{t}}(\boldsymbol{\kappa}_t), \qquad (14)$$

where

$$\breve{E}^{\mathrm{TE}}(\boldsymbol{\kappa}_t, \tau) = \kappa_t^{-1}(\kappa_y \breve{E}_x - \kappa_x \breve{E}_y),$$
$$\breve{E}^{\mathrm{TM}}(\boldsymbol{\kappa}_t, \tau) = (\kappa_z \kappa_t)^{-1}(\kappa_x \breve{E}_x + \kappa_y \breve{E}_y). \qquad (15)$$

By applying the inverse STT in Eq. (7) to Eq. (14), the aperture field in Eq. (1) can be propagated into $z > 0$ half-space in a similar manner to Eq. (10), giving

$$\mathbf{E}(\mathbf{r}, t) = \mathbf{E}^{\mathrm{TE}}(\mathbf{r}, t) + \mathbf{E}^{\mathrm{TM}}(\mathbf{r}, t), \qquad (16)$$

where

$$\mathbf{E}^{\mathrm{TE}}(\mathbf{r}, t) = \mathrm{Re}\left[\frac{-1}{(2\pi c)^2} \int \mathrm{d}^2\kappa_t \hat{\mathbf{n}}(\boldsymbol{\kappa}_t) \partial_t^2 \breve{E}^{\mathrm{TE}}(\boldsymbol{\kappa}_t, t - c^{-1}\hat{\boldsymbol{\kappa}} \cdot \mathbf{r})\right],$$
$$\mathbf{E}^{\mathrm{TM}}(\mathbf{r}, t) = \mathrm{Re}\left[\frac{-1}{(2\pi c)^2} \int \mathrm{d}^2\kappa_t \hat{\mathbf{t}}(\boldsymbol{\kappa}_t) \partial_t^2 \breve{E}^{\mathrm{TM}}(\boldsymbol{\kappa}_t, t - c^{-1}\hat{\boldsymbol{\kappa}} \cdot \mathbf{r})\right]. \quad (17)$$

3. SCALAR FRAME-BASED PULSED-BEAM EXPANSION

A. General Formulation

In order to establish the EM frame-based PB expansion, we briefly review here the main results of the scalar TD frame-based beam decomposition, which was introduced in [8]. The TD beam summation is constructed in the framework of the WRT frames, where the $z = 0$ scalar aperture field $\breve{u}_0(\mathbf{r}_t, t)$ is expanded using a set of WRT functions. The aperture field is assumed to be band-limited in the frequency interval

$$\Omega = (\omega_{\min}, \omega_{\max}). \qquad (18)$$

The PB expansion is constructed over the discrete five-dimensional frame spectral lattice

$$(\bar{x}, \bar{y}, \bar{\kappa}_x, \bar{\kappa}_y, \bar{\tau}) = (N_x \Delta\bar{x}, N_y \Delta\bar{y}, N_{\kappa_x} \Delta\bar{\kappa}_x, N_{\kappa_y} \Delta\bar{\kappa}_y, N_\tau \Delta\bar{\tau}), \quad (19)$$

where $(\Delta\bar{x}, \Delta\bar{y})$ are the unit-cell dimensions in the (x, y) coordinates and $(\Delta\bar{\kappa}_x, \Delta\bar{\kappa}_y)$ and $\Delta\bar{\tau}$ denote the unit-cell dimensions in the spectral variables (κ_x, κ_y) and τ, respectively. We use the index $\mathbf{N} = (N_x, N_y, N_{\kappa_x}, N_{\kappa_y}, N_\tau)$ to tag the lattice points (see Fig. 1). It is convenient to chose equal-direction unit-cell dimensions $\Delta\bar{\kappa}_x = \Delta\bar{\kappa}_y \equiv \Delta\bar{\kappa}$ and equal-space unit-cell dimensions $\Delta\bar{x} = \Delta\bar{y} \equiv \Delta\bar{r}_t$. The unit-cell dimensions should satisfy the overcompleteness criterion

$$\bar{\omega}\Delta\bar{\kappa}\Delta\bar{r}_t = 2\pi c\nu, \qquad (20)$$

where $0 \le \nu \le 1$ is termed the overcompleteness (or oversampling) parameter and $\bar{\omega}$ denotes a reference frequency that is chosen to be greater then $\omega_{\max}$, i.e., $\bar{\omega} = K\omega_{\max}$ with typically $2.5 < K < 3$ [8]. This choice implies a K times overcompleteness (redundancy) of the frame at $\omega_{\max}$, while for lower frequencies the overcompleteness increases like $K\omega_{\max}/\omega$ {see Eqs. (20)–(21) in [3]}. The temporal unit-cell dimension satisfies
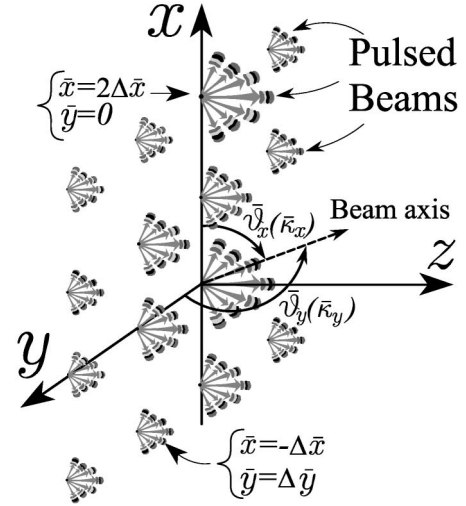
Fig. 1. Discrete frame spectral lattice. The fields in $z \ge 0$ are evaluated by superposition of tilted, shifted, and delayed PBs, which are emanating from the aperture distribution plane over the discrete frame spatial-directional-temporal lattice in Eq. (19). Each beam propagator emanates from a lattice point $(\bar{x}, \bar{y})$, in a direction of $(\vartheta_x, \vartheta_y) = \cos^{-1}[(\bar{\kappa}_x, \bar{\kappa}_y)]$ with respect to the corresponding axis and in delay time of $\bar{\tau}$.

$$\Delta\bar{\tau} < 2\pi/(\omega_{\max} + \omega_h), \qquad (21)$$

where ω_h denotes the maximum frequency of the synthesis and analysis windows that are define next {see Eqs. (13) and (A12) in [8] and the specific example in Eq. (39)}.

Next a synthesis set is defined over the frame lattice. This set is obtained from the synthesis ("mother") window $\psi(\mathbf{r}_t, t)$ via

$$\psi_N(\mathbf{r}_t, t) = \psi[\mathbf{r}_t - \bar{\mathbf{r}}_t, t - \bar{\tau} - c^{-1}\bar{\boldsymbol{\kappa}}_t \cdot (\mathbf{r}_t - \bar{\mathbf{r}}_t)], \qquad (22)$$

were $\bar{\mathbf{r}}_t = (\bar{x}, \bar{y})$ and $\bar{\boldsymbol{\kappa}}_t = (\bar{\kappa}_x, \bar{\kappa}_y)$. Throughout the paper, subscript N denotes an object over the frame spectral lattice in Eq. (19). Similarly, a set of WRT functions is obtained from the analysis ("dual") window, $\varphi(\mathbf{r}_t, t)$, via

$$\varphi_N(\mathbf{r}_t, t) = \varphi[\mathbf{r}_t - \bar{\mathbf{r}}_t, t - \bar{\tau} - c^{-1}\bar{\boldsymbol{\kappa}}_t \cdot (\mathbf{r}_t - \bar{\mathbf{r}}_t)]. \qquad (23)$$

The analysis window can be evaluated from the synthesis one in several ways, which are listed in [8] [see Eq. (38)]. The set in Eq. (22) constitutes a frame that can be used to expand functions of $(\mathbf{r}_t, t)$ [see Eq. (24)]. This frame property is proven in Appendices A and B in [8]. The window function ψ can be quite general, but it is assumed here that it is localized about the origin in the $(\mathbf{r}_t, t)$ plan, such that its spatial width is much greater than its temporal width. As such, ψ_N in Eq. (22) are centered about the frame lattice point $(\mathbf{r}_t, t) = (\bar{\mathbf{r}}_t, \bar{\tau})$ in Eq. (19) and have linear delays whose slant angle is determined by the spectral lattice coordinate $\bar{\boldsymbol{\kappa}}_t$. Because of these properties, ψ_N have the shape of the kernel of a WRT about the point $(\bar{\mathbf{r}}_t, \bar{\tau})$ and therefore the set has been termed the WRT frame.

The WRT frame representation of the scalar aperture field is given by

$$u_0(\mathbf{r}_t, t) = \sum_N a_N \psi_N(\mathbf{r}_t, t), \qquad (24)$$

where the expansion frame set, $\psi_N(\mathbf{r}_t, t)$, is given in Eq. (22). If the window function $\varphi(\mathbf{r}, t)$ is chosen properly, then the sets in Eqs. (23) and (22) constitute a dual frame sets. Because of the overcompleteness of the representation, the coefficient set a_N is not unique and can be calculated in various ways. One option is to use the dual set in Eq. (23). Thus, the expansion coefficients a_N are evaluated by the inner product of the aperture distribution with the analysis set in Eq. (23), namely,

$$a_N = \int \mathrm{d}t \int \mathrm{d}^2 r_t u_0(\mathbf{r}_t, t)\varphi_N(\mathbf{r}_t, t). \qquad (25)$$

Recalling the discussion following Eq. (23), the operation in Eq. (25) has been termed a WRT, which extracts from the aperture field the local (directional) radiation properties.

In order to adjust the scalar theory to the EM vectorial case, it is beneficial to evaluate the frame expansion coefficients directly from the field's PW spectral distribution $\breve{u}_0(\boldsymbol{\kappa}_t, \tau)$ [see Eq. (47)]. First we replace $u_0(\mathbf{r}_t, t)$ in Eq. (25) by its inverse STT

$$u_0(\mathbf{r}_t, t) = \frac{-1}{(2\pi c)^2} \int \mathrm{d}^2\kappa_t \partial_t^2 \tilde{u}_0(\boldsymbol{\kappa}_t, t - c^{-1}\boldsymbol{\kappa}_t \cdot \mathbf{r}_t). \qquad (26)$$

By changing the integration variable to $\tau = t - c^{-1}\boldsymbol{\kappa}_t \cdot \mathbf{r}_t$ and inverting the order of integrations we obtain the desired expression for the expansion coefficients

$$a_N = \frac{-1}{(2\pi c)^2} \int \mathrm{d}\tau \int \mathrm{d}^2\kappa_t \partial_\tau^2 \tilde{u}_0(\boldsymbol{\kappa}_t, \tau)\tilde{\varphi}_N(\boldsymbol{\kappa}_t, \tau), \qquad (27)$$

where

$$\tilde{\varphi}_N(\boldsymbol{\kappa}_t, \tau) = \bar{\tau}\,\tilde{\varphi}(\boldsymbol{\kappa}_t - \bar{\boldsymbol{\kappa}}_t, \tau - \bar{\tau} + c^{-1}\boldsymbol{\kappa}_t \cdot \bar{\mathbf{r}}_t). \qquad (28)$$

The scalar field in $z \geq 0$ due to sources in $z < 0$ is obtained by propagating each $\psi_N(\mathbf{r}_t, t)$ window element in summation Eq. (24) into $z \geq 0$ half-space. Therefore, the frame-based representation of the field is given by

$$u(\mathbf{r}, t) = \sum_N a^N P_N(\mathbf{r}, t), \qquad (29)$$

where each beam propagator, $P_N(\mathbf{r}, t)$, satisfies the scalar wave equation

$$[\nabla^2 - c^{-2}\partial_t^2]P_N(\mathbf{r}, t) = 0, \qquad (30)$$

subject to causality boundary conditions. The beam propagator can be evaluated in several ways, such as TD Green's function (Kirchhoff's) integration [47]

$$P_N(\mathbf{r}, t) = \int \mathrm{d}^2 r_t' \frac{z}{2\pi R^2}(R^{-1} + c^{-1}\partial_t)\psi_N(\mathbf{r}_t', t - R/c), \qquad (31)$$

where $\mathbf{r}_t' = (x', y')$ and $R = \sqrt{(x - x')^2 + (y - y')^2 + z^2}$. Alternative representation is obtained by applying a TD plane-wave spectral decomposition of the form in Eq. (10), i.e., $P_N(\mathbf{r}, t) = \mathrm{Re}\,\breve{P}_N(\mathbf{r}, t)$ with

$$\breve{P}_N(\mathbf{r}, t) = \frac{-1}{(2\pi c)^2} \int \mathrm{d}^2\kappa_t \partial_t^2 \breve{\psi}_N(\boldsymbol{\kappa}_t, t - c^{-1}\hat{\boldsymbol{\kappa}} \cdot \mathbf{r}), \qquad (32)$$

where $\breve{\psi}_N$ denotes the (analytic) TD plane-wave spectrum Eq. (6) of $\breve{\psi}_N(\mathbf{r}_t, t)$

$$\breve{\psi}_N(\boldsymbol{\kappa}_t, \tau) = \int \mathrm{d}^2 r_t \breve{\psi}_N(\mathbf{r}_t, \tau + c^{-1}\boldsymbol{\kappa}_t \cdot \mathbf{r}_t). \qquad (33)$$

By inserting Eq. (22) into Eq. (33), we identify

$$\breve{\psi}_N(\boldsymbol{\kappa}_t, \tau) = \breve{\psi}(\boldsymbol{\kappa}_t - \bar{\boldsymbol{\kappa}}_t, \tau - \bar{\tau} + c^{-1}\boldsymbol{\kappa}_t \cdot \bar{\mathbf{r}}_t). \qquad (34)$$

The spectral representation in Eq. (29) describes the field as a discrete superposition of PB propagators that emanate from points $(\bar{x}, \bar{y})$ on the frame spectral lattice, in a discrete set of directions [that are determine by the spectral wavenumbers $(\bar{\kappa}_x, \bar{\kappa}_y)$] and in a discrete set of delays $\bar{\tau}$ (see Fig. 1). Assuming that $\psi(\mathbf{r}_t, t)$ is a short pulsed window, the spatial-temporal and spectral distributions of ψ_N are localized about $(\mathbf{r}_t, t) = (\bar{\mathbf{r}}_t, \bar{\tau})$ and $(\boldsymbol{\kappa}_t, \tau) = (\bar{\boldsymbol{\kappa}}_t, \bar{\tau} - c^{-1}\bar{\boldsymbol{\kappa}}_t \cdot \bar{\mathbf{r}}_t)$, respectively. Consequently, $\breve{P}_N(\mathbf{r}, t)$ are collimated scalar PB propagators whose axes emerge from the processing-dependent point $\mathbf{r}_t = \bar{\mathbf{r}}_t$ over $z = 0$ plane, at the (processing-dependent) time $t = \bar{\tau}$, and in the (processing-dependent) direction

$$\hat{\bar{\boldsymbol{\kappa}}} = (\bar{\boldsymbol{\kappa}}_t, \bar{\kappa}_z), \quad \bar{\kappa}_z = \sqrt{1 - \bar{\kappa}_t^2}, \qquad (35)$$

where $\bar{\kappa}_t^2 = \bar{\kappa}_x^2 + \bar{\kappa}_y^2$. Propagating PBs occur for $\bar{\kappa}_t < 1 - \Delta_{\kappa_t}$, where Δ_{κ_t} denotes the (plane-wave) spectral width of $\tilde{\psi}(\boldsymbol{\kappa}_t, \tau)$. For $\bar{\kappa}_t > 1 + \Delta_{\kappa_t}$, the spectral distribution is localized in the evanescent spectral range, and the corresponding beam propagators decay with z (see specific examples for pulsed-quadratic windows in Subsection 3.B).

Finally we obtain a frame spectral representation for the TD plane-wave spectrum of the aperture field $\breve{u}_0(\boldsymbol{\kappa}_t, \tau)$, which is required in order to obtain the discrete TE/TM vectorial frame-based representation in the next section. By applying the analytic signal continuation in Eq. (2) to the summation in Eq. (24) and then applying the STT operator in Eq. (33) to the resulting $\breve{u}_0(\mathbf{r}_t, t)$, we obtain, after inverting the order of integration and summation,

$$\breve{u}_0(\boldsymbol{\kappa}_t, \tau) = \sum_N a_N \breve{\psi}_N(\boldsymbol{\kappa}_t, \tau), \qquad (36)$$

where $\tilde{\psi}_N$ is given in Eq. (34) and the expansion coefficients are evaluated from the aperture field via Eq. (25) or (27).

B. Isodiffracting Pulsed-Quadratic Frames
The general frame representation in Subsection 3.A is applied here for the special case of ID pulsed-quadratic synthesis windows [44]. These window functions exhibit frequency-independent collimation (Rayleigh) lengths, they maximize the localization as implied by the uncertainty principle and yield analytically trackable beam-type propagators. Therefore, ID windows have been used extensively for modeling beam propagation [6–8,18,24,27,46].

The ID pulsed-quadratic synthesis spatial and spectral windows are given by

$$\psi(\mathbf{r}_t, t) = \mathrm{Re}[\breve{g}'(t - jr_t^2/2bc)],$$

$$\tilde{\psi}(\boldsymbol{\kappa}_t, \tau) = 2\pi bc\,\mathrm{Im}[\breve{g}(\tau - jb\kappa_t^2/2c)], \qquad (37)$$

where $\breve{g}$ is an analytic function with a frequency band of (ω_l, ω_h) with $\omega_l \le \omega_{\min}$, $\omega_h \ge \omega_{\max}$, b is a real parameter, $r_t^2 = \mathbf{r}_t \cdot \mathbf{r}_t$, and the prime denotes a derivative with respect to the argument. The (temporal) spectrum of $\breve{g}(t)$ equals 1 over the frequency band Ω in (18) where the data resides. The parameter b sets the synthesis window width to the order of $\sqrt{cT_b b}$ where T_b denotes the temporal support of $\breve{g}'(t)$. This parameter determine the beam propagator's collimation distances [see Eq. (44)]. In order to obtain a "snug" frame over the entire frequency band Ω, the collimation distance b should be on the order of $\Delta \bar{r}_t / \Delta \bar{\kappa}$, {For further details, please refer to Eq. (24) in [8] and the discussion thereafter}.

The analysis spatial-temporal window and its PW spectral distribution can be approximated in the high oversampling regime by [8]

$$\varphi(\mathbf{r}_t, t) \simeq -\frac{2}{\bar{\omega}^3 \Delta \bar{r}_t{}^2}\,\mathrm{Im}[\breve{g}''(t - jr_t^2/2bc)],$$

$$\tilde{\varphi}(\boldsymbol{\kappa}_t, \tau) \simeq \frac{4\pi bc}{\bar{\omega}^3 \Delta \bar{r}_t{}^2}\,\mathrm{Re}[\breve{g}'(\tau - jb\kappa_t^2/2c)]. \qquad (38)$$

The frame expansion coefficients can be evaluated directly in the spectral domain by inserting $\tilde{\varphi}(\boldsymbol{\kappa}_t, \tau)$ in Eq. (38) into Eqs. (27) and (28).

In the present investigation, we apply the linearly tapered bandpass filter that was introduced in [8]

$$\breve{g}(t) = \left\{ \frac{1}{\pi jt}[\mathrm{sinc}(\Delta_L t)e^{-j(\omega_L - \Delta_L)t} - \mathrm{sinc}(\Delta_H t)e^{-j(\omega_H + \Delta_H)t}] \right\}, \qquad (39)$$

where $\mathrm{sinc}(t) = \sin t/t$, ω_H and ω_L are the maximum and minimum frequencies of the bandpass and Δ_H, Δ_L denote the tapering frequencies (see [8] Fig. 4). Thus the maximum frequency of the frame windows in Eq. (21) is identified as $\omega_h = \omega_H + 2\Delta_H$.

The paraxial (short-pulsed) asymptotic ID PB propagators that correspond to the synthesis windows in Eq. (37) are obtained by utilizing the local beam coordinates $\mathbf{r}_{b_N} = (x_{b_N}, y_{b_N}, z_{b_N})$ that are defined, for a given spectral point $(\bar{x}, \bar{y}, \bar{\kappa}_x, \bar{\kappa}_y)$ on the frame lattice, by the rotation transformation [7]

$$\begin{pmatrix} x_{b_N} \\ y_{b_N} \\ z_{b_N} \end{pmatrix} = \begin{pmatrix} \cos\bar{\vartheta}_N \cos\bar{\varphi}_N & \cos\bar{\vartheta}_N \sin\bar{\varphi}_N & -\sin\bar{\vartheta}_N \\ -\sin\bar{\varphi}_N & \cos\bar{\varphi}_N & 0 \\ \sin\bar{\vartheta}_N \cos\bar{\varphi}_N & \sin\bar{\vartheta}_N \sin\bar{\varphi}_N & \cos\bar{\vartheta}_N \end{pmatrix}$$

$$\times \begin{pmatrix} x - \bar{x} \\ y - \bar{y} \\ z \end{pmatrix}, \qquad (40)$$

where $(\bar{\vartheta}_N, \bar{\varphi}_N)$ are the spherical angles that define the spectral unit vector $\hat{\bar{\boldsymbol{\kappa}}}$ in Eq. (35), i.e.,

$$\cos\bar{\vartheta}_N = \bar{\kappa}_z, \qquad \cos\bar{\varphi}_N = \bar{\kappa}_x/\bar{\kappa}_t, \qquad \sin\bar{\varphi}_N = \bar{\kappa}_y/\bar{\kappa}_t. \quad (41)$$

Thus, on-axis observation points, for which

$$\mathbf{r}_t - \bar{\mathbf{r}}_t = z\tan\bar{\vartheta}_N(\cos\bar{\varphi}_N\hat{\mathbf{x}} + \sin\bar{\varphi}_N\hat{\mathbf{y}}), \qquad (42)$$

are identified by $x_{b_N} = y_{b_N} = 0$. By utilizing the beam coordinates, the PB propagators are evaluated asymptotically by

$$P_N(\mathbf{r}, t) \sim \mathrm{Re}\left[\sqrt{\frac{-jF_{N_1}}{z_{b_N} - jF_{N_1}}\frac{-jF_{N_2}}{z_{b_N} - jF_{N_2}}} \right.$$

$$\left. \times \breve{g}'\left(t - \bar{\tau} - \frac{z_{b_N}}{c} - \frac{x_{b_N}^2/2c}{z_{b_N} - jF_{N_1}} - \frac{y_{b_N}^2/2c}{z_{b_N} - jF_{N_2}} \right) \right]. \qquad (43)$$

The PBs waists are located at $z_{b_N} = 0$ with collimation distances of

$$F_{N_1} = b\cos^2\bar{\vartheta}_N, \qquad F_{N_2} = b, \qquad (44)$$

in x_{b_N} and y_{b_N}, respectively.

4. VECTORIAL EM FIELD DECOMPOSITION

In order to obtain a TE/TM frame-based representation of the electric field, $\mathbf{E}(\mathbf{r}, t)$, we introduce the TE/TM coefficients

$$a_N^{\mathrm{TE/TM}} = \int \mathrm{d}t \int \mathrm{d}^2 r_t E^{\mathrm{TE/TM}}(\mathbf{r}_t, t)\varphi_N(\mathbf{r}_t, t), \qquad (45)$$

where φ_N are the analysis set in Eq. (23) and E^{TE} and E^{TM} are obtained by applying the inverse STT in Eq. (7) to the spectral distributions in Eq. (17), i.e.,

$$E^{\mathrm{TE/TM}}(\mathbf{r}_t, t) = \frac{-1}{(2\pi c)^2}\int \mathrm{d}^2\kappa_t \partial_t^2 \tilde{E}^{\mathrm{TE/TM}}(\boldsymbol{\kappa}_t, t - c^{-1}\boldsymbol{\kappa}_t \cdot \mathbf{r}_t). \quad (46)$$

It is beneficial to evaluate these coefficients directly from the PW spectral distributions in Eq. (15) without evaluating the TE/TM aperture fields. By applying the formulation in Eq. (27) to either a_N^{TE} or a_N^{TM} in Eq. (45), we obtain

$$a_N^{\mathrm{TE/TM}} = \frac{-1}{(2\pi c)^2}\int \mathrm{d}\tau \int \mathrm{d}^2\kappa_t \partial_\tau^2 \tilde{E}^{\mathrm{TE/TM}}(\boldsymbol{\kappa}_t, \tau)\tilde{\varphi}_N(\boldsymbol{\kappa}_t, \tau), \quad (47)$$

where the spectral distributions $\tilde{E}^{\mathrm{TE}}$ and $\tilde{E}^{\mathrm{TM}}$ are given in Eq. (15) and $\tilde{\varphi}_N$ is given in Eq. (28). Thus, by using Eq. (36) for each TE/TM electric field spectral component, we can write

$$\breve{E}^{\mathrm{TE/TM}}(\boldsymbol{\kappa}_t, \tau) = \sum_N a_N^{\mathrm{TE/TM}}\breve{\psi}_N(\boldsymbol{\kappa}_t, \tau), \qquad (48)$$

where $\breve{\psi}_N(\boldsymbol{\kappa}_t, \tau)$ are given in Eq. (34).

The expansion coefficients in Eq. (45) are used next in order to obtained a frame-based spectral representation for the TE/TM electric fields in $z \ge 0$. By inserting Eq. (48) into Eq. (17) and inverting the order of integration and summation, we obtain, for each field component in Eq. (16),

$$\mathbf{E}^{\mathrm{TE/TM}}(\mathbf{r}, t) = \sum_N a_N^{\mathrm{TE/TM}}\mathbf{E}_N^{\mathrm{TE/TM}}(\mathbf{r}, t), \qquad (49)$$

where $\mathbf{E}_N^{\mathrm{TE/TM}} = \mathrm{Re}\,\breve{\mathbf{E}}_N^{\mathrm{TE/TM}}$ with

$$\breve{\mathbf{E}}_N^{\text{TE}}(\mathbf{r}, t) = \frac{-1}{(2\pi c)^2} \int d^2 \kappa_t \partial_t^2 \hat{\mathbf{n}}(\boldsymbol{\kappa}_t) \breve{\psi}_N(\boldsymbol{\kappa}_t, t - c^{-1} \hat{\boldsymbol{\kappa}} \cdot \mathbf{r}),$$

$$\breve{\mathbf{E}}_N^{\text{TM}}(\mathbf{r}, t) = \frac{-1}{(2\pi c)^2} \int d^2 \kappa_t \partial_t^2 \hat{\mathbf{t}}(\boldsymbol{\kappa}_t) \breve{\psi}_N(\boldsymbol{\kappa}_t, t - c^{-1} \hat{\boldsymbol{\kappa}} \cdot \mathbf{r}), \quad (50)$$

denoting the analytic TE/TM electric field of the *EM PB propagators* over the frame spectral lattice in Eq. (19). For short-pulsed $\psi(\mathbf{r}_t, t)$ windows, $\mathbf{E}_N^{\text{TE}}$ and $\mathbf{E}_N^{\text{TM}}$ are collimated EM PB propagators whose axes emerge from the space–time point $(\mathbf{r}_t, t) = (\bar{\mathbf{r}}_t, \bar{\tau})$ over the $z = 0$ plane, in the direction $\hat{\boldsymbol{\kappa}}$ in Eq. (35).

Equations (16), (49), and (50) represent the electric field $\mathbf{E}(\mathbf{r}, t)$ as a discrete superposition of EM PB waveobjects, $\mathbf{E}_N^{\text{TE}}$ and $\mathbf{E}_N^{\text{TM}}$, which are exact solutions of Maxwell's equations. The excitation amplitudes of these EM propagators, a_N^{TE} and a_N^{TM}, are obtained from the aperture field spectral distribution $\tilde{\mathbf{E}}_t$ via Eqs. (47) and (15). The EM PB propagators are characterized by both transversal and longitudinal localization and high directivity. Each of these propagators consists of only TE or TM polarizations thus they are pure TE/TM EM propagators.

In order to gain insight on the structure of the EM PB propagators, we note that in the short-pulsed regime $\hat{\mathbf{n}}(\boldsymbol{\kappa}_t)$ and $\hat{\mathbf{t}}(\boldsymbol{\kappa}_t)$ in the integrand of Eq. (50) are sampled at the on-axis stationary point $\boldsymbol{\kappa}_t = \bar{\boldsymbol{\kappa}}_t$ [7] (see also [46]). Hence, the resulting plane-wave spectral integrals can be evaluated asymptotically by

$$\mathbf{E}_N^{\text{TE}}(\mathbf{r}, t) \sim \hat{\mathbf{n}}(\bar{\boldsymbol{\kappa}}_t) P_N(\mathbf{r}, t), \qquad \mathbf{E}_N^{\text{TM}}(\mathbf{r}, t) \sim \hat{\mathbf{t}}(\bar{\boldsymbol{\kappa}}_t) P_N(\mathbf{r}, t), \quad (51)$$

where $\hat{\mathbf{n}}$ and $\hat{\mathbf{t}}$ are defined in Eq. (13) and $P_N(\mathbf{r}, t)$ is the (short-pulsed) asymptotic evaluation of the scalar PB propagators in Eq. (32). Each of the EM PB propagators in Eq. (51) is either TE or TM polarized with respect to the beam axis direction that is determined via Eq. (35) by the frame spectral directional variable $\bar{\boldsymbol{\kappa}}_t$.

The TE/TM ID pulsed-quadratic beam propagators that are corresponding to the windows in Eq. (37) are obtained by inserting $\breve{\psi}_N$ in Eq. (34) with Eq. (37) into Eq. (50). The resulting plane-wave spectral integrals can be evaluated asymptotically in the short-pulsed regime by inserting the scalar ID PB propagator in Eq. (43) into Eq. (51).

The magnetic field in $z \geq 0$ is obtained by applying Faraday's law, $\mathbf{H} = (-j\omega\mu_0)^{-1} \nabla \times \mathbf{E}$, to Eq. (49) and inserting Eq. (50). Thus,

$$\mathbf{H}(\mathbf{r}, t) = \mathbf{H}^{\text{TE}}(\mathbf{r}, t) + \mathbf{H}^{\text{TM}}(\mathbf{r}, t), \quad (52)$$

with

$$\mathbf{H}^{\text{TE/TM}}(\mathbf{r}, t) = \sum_N a_N^{\text{TE/TM}} \mathbf{H}_N^{\text{TE/TM}}(\mathbf{r}, t), \quad (53)$$

where $\mathbf{H}_N^{\text{TE}}$ and $\mathbf{H}_N^{\text{TM}}$ denote the magnetic fields of the TE/TM EM beam propagators and a_N^{TE} and a_N^{TM} are given in Eq. (47). These magnetic fields can be evaluated by applying the well-known plane-wave spectral relation $\tilde{\mathbf{H}} = \eta_0^{-1} \hat{\boldsymbol{\kappa}} \times \tilde{\mathbf{E}}$ to Eq. (50). Thus $\mathbf{H}_N^{\text{TE/TM}} = \text{Re } \breve{\mathbf{H}}_N^{\text{TE/TM}}$ where the analytic magnetic fields are given by the spectral representation

$$\breve{\mathbf{H}}_N^{\text{TE}}(\mathbf{r}, t) = \frac{1}{\eta_0} \frac{-1}{(2\pi c)^2} \int d^2 \kappa_t \hat{\mathbf{t}}(\boldsymbol{\kappa}_t) \partial_t^2 \breve{\psi}_N(\boldsymbol{\kappa}_t, t - c^{-1} \hat{\boldsymbol{\kappa}} \cdot \mathbf{r}),$$

$$\breve{\mathbf{H}}_N^{\text{TM}}(\mathbf{r}, t) = \frac{1}{\eta_0} \frac{1}{(2\pi c)^2} \int d^2 \kappa_t \hat{\mathbf{n}}(\boldsymbol{\kappa}_t) \partial_t^2 \breve{\psi}_N(\boldsymbol{\kappa}_t, t - c^{-1} \hat{\boldsymbol{\kappa}} \cdot \mathbf{r}), \quad (54)$$

where $\eta_0 = \sqrt{\mu_0/\epsilon_0}$ is the free-space impedance, the spectral unit-vectors $\hat{\mathbf{n}}$ and $\hat{\mathbf{t}}$ are given in Eq. (13), and $\tilde{\psi}_N$ is the spectral synthesis set in Eq. (34).

Following the discussion preceding Eq. (51), the short-pulsed asymptotic magnetic fields take the form

$$\mathbf{H}_N^{\text{TE}}(\mathbf{r}, t) \sim \eta_0^{-1} \hat{\mathbf{t}}(\bar{\boldsymbol{\kappa}}_t) P_N(\mathbf{r}, t), \quad \mathbf{H}_N^{\text{TM}}(\mathbf{r}, t) \sim \eta_0^{-1} \hat{\mathbf{n}}(\bar{\boldsymbol{\kappa}}_t) P_N(\mathbf{r}, t), \quad (55)$$

where $\hat{\mathbf{n}}$ and $\hat{\mathbf{t}}$ are defined in Eq. (13) and $P_N(\mathbf{r}, t)$ is the (short-pulsed) asymptotic evaluation of the PB scalar propagator in Eq. (32) that is given in closed form for ID pulsed-quadratic windows in Eq. (43).

5. ILLUSTRATIVE EXAMPLE

In the example presented here, we apply the expansion procedure in Eq. (49) and demonstrate the numerical considerations in obtaining the TE/TM frame-coefficients.

A. Aperture Field
The EM field in this example is in the form of an x-polarized complex source PB (CSPB) [50] which is given by

$$\mathbf{E}(\mathbf{r}, t) = \text{Re } V_0 \frac{\breve{f}(t_d)}{4\pi R} \hat{\mathbf{x}},$$

$$R = \left[x^2 + y^2 + (z - z' - jb_z')^2 \right]^{\frac{1}{2}},$$

$$t_d = t - t' - R/c, \quad (56)$$

where t' and $z' < 0$ denote the delay and location parameters of the complex source, $b_z' > 0$ is a real parameter, $\breve{f}(t)$ is some analytic signal and $V_0 = 1$ volt is added to adjust for the physical units. By properly choosing $\breve{f}(t)$, one can achieve a well localized field in space–time with a limited bandwidth, as required in Eq. (18). In the present example, we used

$$\breve{f}(t) = e^{-j\omega_c t} \left[2 \text{sinc}\left(\frac{2\pi t}{T}\right) + \text{sinc}\left(\frac{2\pi(t - T/2)}{T}\right) \right. $$
$$\left. + \text{sinc}\left(\frac{2\pi(t + T/2)}{T}\right) \right], \quad (57)$$

where $\text{sinc } x = \sin x / x$. This pulse corresponds to a derivative of the modulated "raised-cosine filter" (with roll-off factor 1). This choice set the bandwidth $\Omega = (\omega_c - 2\pi/T, \omega_c + 2\pi/T)$.

In this example, the modulated frequency $\omega_c = 15T^{-1}$, and thus $\Omega = [\omega_{\min}, \omega_{\max}] = [(15 - 2\pi)/T, (15 + 2\pi)/T]$. All the temporal parameters are normalized with respect to T, which is the typical illumination time of the aperture field and spatial parameters are normalized with respect to cT. The complex source parameters are $z' = -2cT$, $b_z' = 0.3cT$ and $t' = -2T$. The aperture is a $8cT \times 8cT$ square.

The aperture field is obtained by setting $z = 0$ in Eq. (56) with $\breve{f}(t)$ in Eq. (57). The aperture electric field component E_x is plotted in Fig. 2 for $t = 0$. The figure demonstrates the locality of the aperture field.
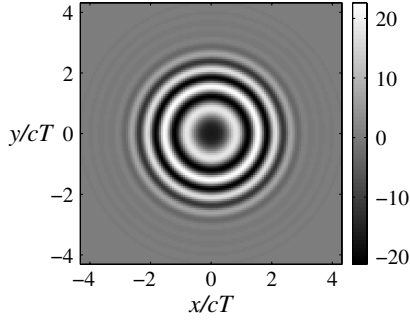
Fig. 2.   Aperture electric field E_x in Eq. (56) over $z = 0$ plane at $t = 0$.

B. Implementation of the STT
The numerical implementation of the STT in Eq. (6) is necessary in order to obtain the TE/TM PW spectral distributions in Eq. (6) and the expansion coefficients in Eq. (15). We implement the STT of $E_x(\mathbf{r}_t, t)$ via

$$\tilde{E}_x(\boldsymbol{\kappa}_t, \tau) = \int \mathrm{d}t \int \mathrm{d}^2 r_t E_x(\mathbf{r}_t, t) \delta(t - \tau - c^{-1} \boldsymbol{\kappa}_t \cdot \mathbf{r}_t). \qquad (58)$$

In Eq. (58), for each $(\boldsymbol{\kappa}_t, \tau)$ the integration is performed over a tilted plane, which is defined by $t = \tau + c^{-1} \boldsymbol{\kappa}_t \cdot \mathbf{r}_t$. In this implementation some interpolation is necessary in order to adjust tilted plane to the rectangular grid of the sampled field $E_x(\mathbf{r}_t, t)$. Here the interpolation is implemented by replacing
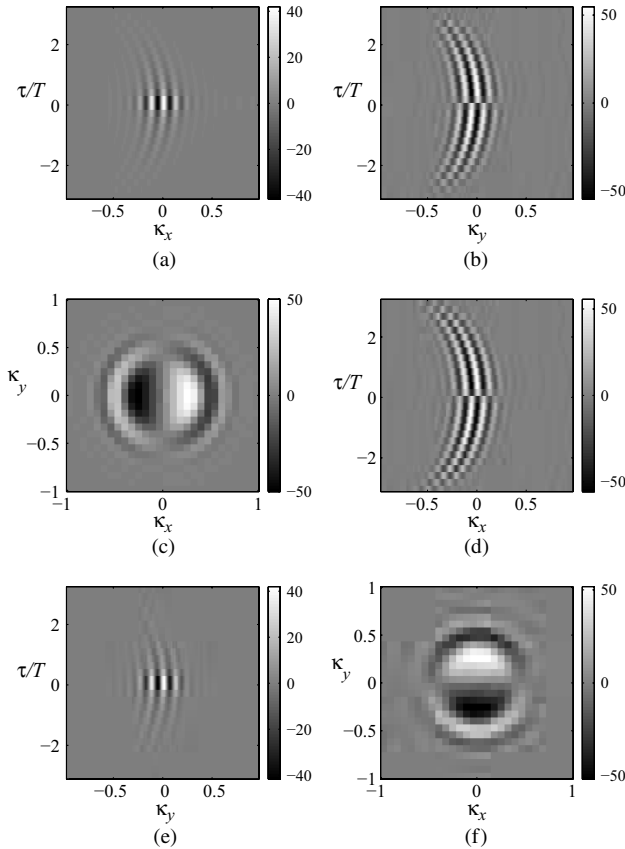
Fig. 3.   TE and TM spectral distributions of the aperture field. $\tilde{E}^{\mathrm{TE}}(\boldsymbol{\kappa}_t, \tau)$ distribution in (a) (κ_x, τ) plane for $\kappa_y = 0$, (b) (κ_y, τ) plane for $\kappa_x = 0$, and (c) (κ_x, κ_y) plane for $\tau = 0$. (d)–(f) are the same as (a)–(c) for the $\tilde{E}^{\mathrm{TM}}$ distribution.
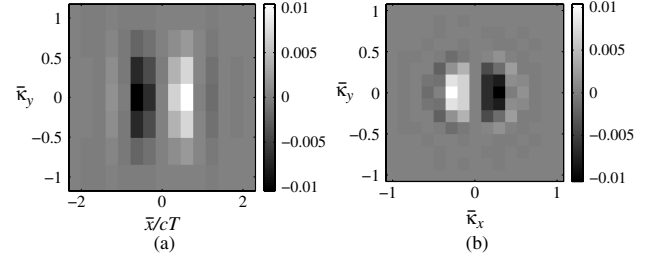
Fig. 4.   TE expansion coefficients a_N^{TE} in various planes: (a) in $(\bar{x}, \bar{\kappa}_y)$ plane for $\bar{y} = \bar{\kappa}_x = \bar{\tau} = 0$ and (b) in $(\bar{\kappa}_x, \bar{\kappa}_y)$ plane for $\bar{x} = \bar{y} = \bar{\tau} = 0$.

$\delta(t)$ in the second equation in Eq. (58) with the weighted δ function, $\delta_w(t)$. In the present example, the weighted δ-function is numerically modeled by a Lorenzian pulse of

$$\delta_w(t) = \frac{1}{\pi} \frac{T_w/2}{t^2 + (T_w/2)^2}, \qquad (59)$$

where the temporal pulse width T_w was set to be the temporal grid unit cell.

Figure 3 presents the TE/TM spectral distributions in Eq. (15) for the aperture field in Eq. (56). $\tilde{E}^{\mathrm{TE}}(\boldsymbol{\kappa}_t, \tau)$ distribution is plotted in (κ_x, τ) plane for $\kappa_y = 0$ in Fig. 3(a), in (κ_y, τ) plane for $\kappa_x = 0$ in Fig. 3(b), and in (κ_x, κ_y) plane for $\tau = 0$ in Fig. 3(c). Figures 3(d), 3(e), and 3(f) are the same as 3(a), 3(b), and 3(c) for the $\tilde{E}^{\mathrm{TM}}$ distribution. The figures show that the spectral distributions resides mainly in the visible spectrum range where $\kappa_t \leq 1$. One can identify the spectral localization of the CSPB field in both the directional and the temporal spectral variables about $(\boldsymbol{\kappa}_t, \tau) = (0, 0)$.

C. Expansion Coefficients
The TE/TM coefficients of the aperture field in Eq. (56) are evaluated by numerical implementation of the integration in Eq. (47). The spectral analysis window, $\breve{\varphi}$ is obtained by inserting the ID pulsed-quadratic window in Eq. (38) with $\breve{g}$ in Eq. (39) into Eq. (28). The window parameters are $b = 10cT$, $\Delta_H = \Delta_L = \omega_{\max}/8$ and $\omega_{L,H} = \omega_{\min,\max} \mp 2\Delta_{L,H}$. The frame spectral grid is set to $\Delta \bar{r}_t = 0.72cT$, $\Delta \bar{\kappa} = 0.14$ and, according to Eq. (21), $\Delta \bar{\tau} = 0.13T$. The overcompleteness parameter in Eq. (20) was set to $\nu = 0.35$. The corresponding spectral frame grid $(N_x, N_y, N_{\bar{\kappa}_x}, N_{\bar{\kappa}_y}, N_{\bar{\tau}})$ size is $7 \times 7 \times 15 \times 15 \times 15$.

The resulting TE and TM coefficients are plotted in Figs. 4 and 5, respectively, for various spectral planes as indicated in the figure captions. Note that the spectral coefficients are confined mainly to the propagating range $\bar{\kappa}_x^2 + \bar{\kappa}_y^2 \leq 1$ and to $\sqrt{\bar{x}^2 + \bar{y}^2} < 2cT$.
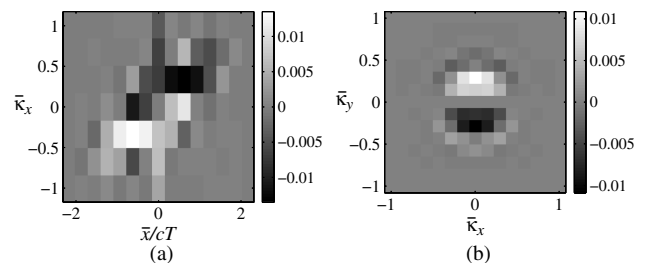
Fig. 5.   TM expansion coefficients a_N^{TM} in various planes: (a) in $(\bar{x}, \bar{\kappa}_x)$ plane for $\bar{y} = \bar{\kappa}_y = \bar{\tau} = 0$ and (b) in $(\bar{\kappa}_x, \bar{\kappa}_y)$ plane for $\bar{x} = \bar{y} = \bar{\tau} = 0$.
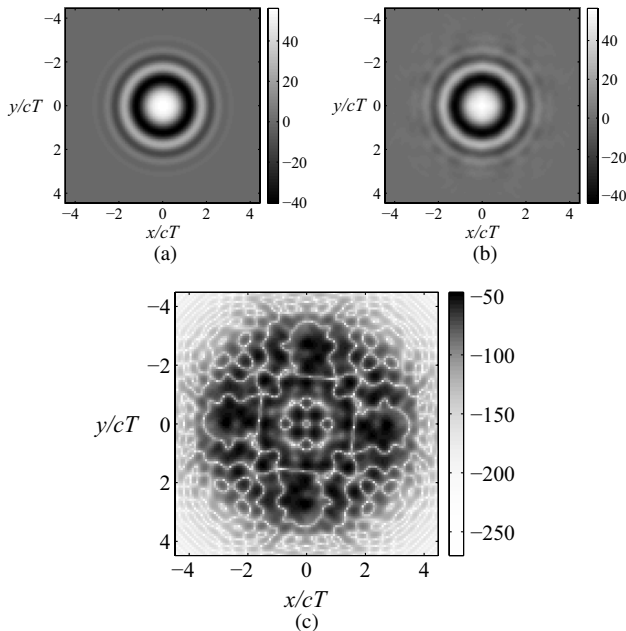
Fig. 6.   Propagating field $E_x(\mathbf{r}, t)$ for $z = 2cT$ and $t = 2T$. (a) Reference field in Eq. (56). (b) Synthesized field. (c) Error in the reconstruction.

D. Field Synthesis

The TE and TM electric fields were synthesized via the summation in Eq. (49) over the TE/TM asymptotic PB propagators in Eqs. (51) and (43) over $z = 2cT$ plane at $t = 2cT$. In order to compare the resulting fields with the reference analytic solution in Eq. (56), we sum over the x components of $\mathbf{E}^{\mathrm{TE}}$ and $\mathbf{E}^{\mathrm{TM}}$. The reference field is plotted in Fig. 6(a), and the synthesized field is plotted in Fig. 6(b). The absolute value of the difference of the synthesized and the reference fields with respect to the maximum reference PB field in dB is plotted in Fig. 6(c). The figure shows that the error is less than –50 dB for all observation points.

6. SUMMARY

Application of an exact beam-type expansion to TD EM aperture fields was introduced, in which the EM PB propagators are *a priori* decomposed into TE and TM fields with respect to constant z planes. This procedure is essential for applying Maxwell's boundary conditions for solving different scattering problems. In Eqs. (49) and (53), the propagating EM field is described as a discrete superposition of the TE and TM EM PB propagators that are defined in Eqs. (50) and (54). The EM PB propagators are shifted, tilted and delayed to points and directions according to the frame spatial-directional-temporal frame lattice in Eq. (19). These vector waveobjects can be obtained asymptotically in the short-pulsed regime from the scalar PB propagators in Eq. (43) via Eqs. (51) and (55).

REFERENCES

1. B. Steinberg, E. Heyman, and L. Felsen, "Phase space beam summation for time-harmonic radiation from large apertures," J. Opt. Soc. Am. A **8**, 41–59 (1991).
2. J. Arnold, "Rays, beams and diffraction in a discrete phase space: Wilson bases," Opt. Express **10**, 716–727 (2002).
3. A. Shlivinski, E. Heyman, A. Boag, and C. Letrou, "A phase-space beam summation formulation for ultra wideband radiation," IEEE Trans. Antennas Propag. **52**, 2042–2056 (2004).
4. A. Shlivinski, E. Heyman, and A. Boag, "A phase-space beam summation formulation for ultrawide-band radiation—Part II: A multiband scheme," IEEE Trans. Antennas Propag. **53**, 948–957 (2005).
5. M. Katsav and E. Heyman, "Phase space Gaussian beam summation analysis of half plane diffraction," IEEE Trans. Antennas Propag. **55**, 1535–1545 (2007).
6. B. Steinberg, E. Heyman, and L. Felsen, "Phase space beam summation for time dependent radiation from large apertures: continuous parametrization," J. Opt. Soc. Am. A **8**, 943–958 (1991).
7. T. Melamed, "Phase-space beam summation: a local spectrum analysis for time-dependent radiation," J. Electromagn. Waves Appl. **11**, 739–773 (1997).
8. A. Shlivinski, E. Heyman, and A. Boag, "A pulsed beam summation formulation for short pulse radiation based on windowed Radon transform (WRT) frames," IEEE Trans. Antennas Propag. **53**, 3030–3048 (2005).
9. A. Shlivinski and E. Heyman, "Windowed Radon transform frames," Appl. Comput. Harmon. Anal. **26**, 322–343 (2009).
10. Y. Gluk and E. Heyman, "Pulsed beams expansion algorithms for time-dependent point-source radiation. A basic algorithm and a standard-pulsed-beams algorithm," IEEE Trans. Antennas Propag. **59**, 1356–1371 (2011).
11. Y. Hadad and T. Melamed, "Non-orthogonal domain parabolic equation and its Gaussian beam solutions," IEEE Trans. Antennas Propag. **58**, 1164–1172 (2010).
12. Y. Hadad and T. Melamed, "Parameterization of the tilted Gaussian beam waveobjects," Prog. Electromagn. Res. **102**, 65–80 (2010).
13. Y. Hadad and T. Melamed, "Time-dependent tilted pulsed-beams and their properties," IEEE Trans. Antennas Propag. **59**, 3855–3862 (2011).
14. S. Shin and L. Felsen, "Gaussian beams in anisotropic media," Appl. Phys. **5**, 239–250 (1974).
15. R. Simon and N. Mukunda, "Shape-invariant anisotropic Gaussian Schell-model beams: a complete characterization," J. Opt. Soc. Am. A **15**, 1361–1370 (1998).
16. I. Tinkelman and T. Melamed, "Gaussian beam propagation in generic anisotropic wavenumber profiles," Opt. Lett. **28**, 1081–1083 (2003).
17. I. Tinkelman and T. Melamed, "Local spectrum analysis of field propagation in anisotropic media. Part I—Time-harmonic fields," J. Opt. Soc. Am. A **22**, 1200–1207 (2005).
18. I. Tinkelman and T. Melamed, "Local spectrum analysis of field propagation in anisotropic media. Part II—Time-dependent fields," J. Opt. Soc. Am. A **22**, 1208–1215 (2005).
19. T. Melamed and L. Felsen, "Pulsed beam propagation in lossless dispersive media. Part I: Theory," J. Opt. Soc. Am. A **15**, 1268–1276 (1998).
20. T. Melamed and L. Felsen, "Pulsed beam propagation in lossless dispersive media. Part II: A numerical example," J. Opt. Soc. Am. A **15**, 1277–1284 (1998).
21. T. Melamed and L. B. Felsen, "Pulsed beam propagation in dispersive media via pulsed plane wave spectral decomposition," IEEE Trans. Antennas Propag. **48**, 901–908 (2000).
22. V. Ĉerveny, M. M. Popov, and I. Pšenĉik, "Computation of wave fields in inhomogeneous media—Gaussian beam approach," Geophys. J. Roy. Astron. Soc **70**, 109–128 (1982).
23. B. W. A. N. Norris and J. Schrieffer, "Gaussian wave packets in inhomogeneous media with curved interfaces," Proc. R. Soc. Lond. **412**, 93–123 (1987).
24. E. Heyman, "Pulsed beam propagation in an inhomogeneous medium," IEEE Trans. Antennas Propag. **42**, 311–319 (1994).
25. F. Bass and L. Resnick, "Wave beam propagation in layered media," Prog. Electromagn. Res. **38**, 111–123 (2002).
26. T. Melamed, "Phase-space Green's functions for modeling time-harmonic scattering from smooth inhomogeneous objects," J. Math. Phys. **45**, 2232–2246 (2004).
27. T. Melamed, "Time-domain phase-space Green's functions for inhomogeneous media," in *Ultrawideband/Short Pulse Electromagnetics 6*, E. L. Mokole, M. Kragalott, K. R. Gerlach, M. Kragalott, and K. R. Gerlach, eds. (Springer-Verlag, 2007), pp. 56–63.
28. Y. Hadad and T. Melamed, "Tilted Gaussian beam propagation in inhomogeneous media," J. Opt. Soc. Am. A **27**, 1840–1850 (2010).

29. H. Chou, P. Pathak, and R. Burkholder, "Application of Gaussian-ray basis functions for the rapid analysis of electromagnetic radiation from reflector antennas," IEE Proc. Microw. Antennas Propag. **150**, 177–183 (2003).

30. H. Chou, P. Pathak, and R. Burkholder, "Novel Gaussian beam method for the rapid analysis of large reflector antennas," IEEE Trans. Antennas Propag. **49**, 880–893 (2001).

31. H.-T. Chou and P. Pathak, "Fast Gaussian beam based synthesis of shaped reflector antennas for contoured beam applications," IEE Proc. Microw. Antennas Propag. **151**, 13–20 (2004).

32. R. Collin, "Scattering of an incident Gaussian beam by a perfectly conducting rough surface," IEEE Trans. Antennas Propag. **42**, 70–74 (1994).

33. O. Kilic and R. Lang, "Scattering of a pulsed beam by a random medium over ground," J. Electromagn. Waves Appl. **15**, 481–516 (2001).

34. G. Gordon, E. Heyman, and R. Mazar, "A phase-space Gaussian beam summation representation of rough surface scattering," J. Acoust. Soc. Am. **117**, 1911–1921 (2005).

35. G. Gordon, E. Heyman, and R. Mazar, "Phase space beam summation analysis of rough surface waveguide," J. Acoust. Soc. Am. **117**, 1922–1932 (2005).

36. T. Melamed, E. Heyman, and L. Felsen, "Local spectral analysis of short-pulse-excited scattering from weakly inhomogenous media: Part I–forward scattering," IEEE Trans. Antennas Propag. **47**, 1208–1217 (1999).

37. T. Melamed, E. Heyman, and L. Felsen, "Local spectral analysis of short-pulse-excited scattering from weakly inhomogeneous media: Part II–inverse scattering," IEEE Trans. Antennas Propag. **47**, 1218–1227 (1999).

38. V. Galdi, H. Feng, D. Castanon, W. Karl, and L. Felsen, "Moderately rough surface underground imaging via short-pulse quasi-ray Gaussian beams," IEEE Trans. Antennas Propag. **51**, 2304–2318 (2003).

39. T. Melamed, "On localization aspects of frequency-domain cattering from low-contrast objects," IEEE Antennas Wireless Propag. Lett. **2**, 40–42 (2003).

40. R. Nowack, S. Dasgupta, G. Schuster, and J.-M. Sheng, "Correlation migration using Gaussian beams of scattered teleseismic body waves," Bull. Seismol. Soc. Am. **96**, 1–10 (2006).

41. M. Popov, N. Semtchenok, P. Popov, and A. Verdel, "Depth migration by the Gaussian beam summation method," Geophysics **75**, S81–S93 (2010).

42. N. Bleistein and S. Gray, "Amplitude calculations for 3D Gaussian beam migration using complex-valued traveltimes," Inverse Probl. **26**, 085017 (2010).

43. T. Melamed, "TE and TM beam decomposition of time-harmonic electromagnetic waves," J. Opt. Soc. Am. A **28**, 401–409 (2011).

44. E. Heyman and T. Melamed, "Certain considerations in aperture synthesis of ultrawideband/short-pulse radiation," IEEE Trans. Antennas Propag. **42**, 518–525 (1994).

45. T. Melamed, "Exact Gaussian beam expansion of time-harmonic electromagnetic waves," J. Electromagn. Waves Appl. **23**, 975–986 (2009).

46. T. Melamed, "Pulsed beam expansion of electromagnetic aperture fields," Prog. Electromagn. Res. **114**, 317–332 (2011).

47. E. Heyman and T. Melamed, *Space-Time Representation of Ultra Wideband Signals* (Elsevier, 1998), pp. 1–63.

48. C. Chapman, "A new method for computing synthetic seismograms," Geophys. J. Roy. Astron. Soc. **54**, 481–518 (1978).

49. R. Martínez-Herrero, P. Mejías, S. Bosch, and A. Carnicer, "Vectorial structure of nonparaxial electromagnetic beams," J. Opt. Soc. Am. A **18**, 1678–1680 (2001).

50. E. Heyman and L. Felsen, "Complex source pulsed beam fields," J. Opt. Soc. Am. A **6**, 806–817 (1989).